Applied Surface Science 265 (2013) 731–737

Contents lists available at SciVerse ScienceDirect

Applied Surface Science

journal homepage: www.elsevier.com/locate/apsusc

Microstructure and surface properties of lignocellulosic-based activated carbons

P. González-García[a,*], T.A. Centeno[b], E. Urones-Garrote[c], D. Ávila-Brande[a], L.C. Otero-Díaz[a]

[a] Departamento de Química Inorgánica, Facultad de Ciencias Químicas, Universidad Complutense, E-28040, Madrid, Spain
[b] Instituto Nacional del Carbón–CSIC, Apartado 73, E-33080 Oviedo, Spain
[c] Centro Nacional de Microscopía Electrónica, Universidad Complutense, E-28040, Madrid, Spain

ARTICLE INFO

Article history:
Received 19 September 2012
Received in revised form
15 November 2012
Accepted 17 November 2012
Available online 23 November 2012

Keywords:
Activated carbons
Transmission Electron Microscopy
Pore structure
Electrochemical Double Layer Capacitor

ABSTRACT

Low cost activated carbons have been produced via chemical activation, by using KOH at 700 °C, from the bamboo species *Guadua Angustifolia* and *Bambusa Vulgaris Striata* and the residues from shells of the fruits of *Castanea Sativa* and *Juglans Regia* as carbon precursors. The scanning electron microscopy micrographs show the conservation of the precursor shape in the case of the *Guadua Angustifolia* and *Bambusa Vulgaris Striata* activated carbons. Transmission electron microscopy analyses reveal that these materials consist of carbon platelet–like particles with variable length and thickness, formed by highly disordered graphene–like layers with sp^2 content ≈ 95% and average mass density of 1.65 g/cm^3 (25% below standard graphite). Textural parameters indicate a high porosity development with surface areas ranging from 850 to 1100 m^2/g and average pore width centered in the supermicropores range (1.3–1.8 nm). The electrochemical performance of the activated carbons shows specific capacitance values at low current density (1 mA/cm^2) as high as 161 F/g in the *Juglans Regia* activated carbon, as a result of its textural parameters and the presence of pseudocapacitance derived from surface oxygenated acidic groups (mainly quinones and ethers) identified in this activated carbon.

1. Introduction

Nowadays there are many studies on the search and development of eco–friendly and low–cost carbon materials, with special attention to those that represent a potential use for the recycling of different types of agro–industrial residues [1,2]. In this sense, production of activated carbon (AC) via thermo–chemical processes from renewable natural resources with high biomass content is feasible [3].

Several AC have been widely prepared and their chemical, textural and physical properties have been studied. Their specific characteristics such as high surface area, pore structure and chemical polarity [4] depend on several factors, mainly the raw material and the activation processes (physical, chemical or combined) making them potential candidates for versatile applications such as adsorbents of heavy metals [5], dyes [6], purification systems for air and water sources [7,8], gas storage [9], support for catalyst reactions [10], batteries [11] and electrode materials [12,13] for electrochemical double layer capacitors (EDLC).

EDLC have been recognized as efficient high power energy devices in electric energy storage and transport as result of their better rate capability and longer cycle life in comparison with batteries and conventional capacitors [14]. AC containing a well defined pore structure, high specific surface area and stable physicochemical characteristics have been intensively studied as electrode materials of EDLC [15,16]. Although superior capacity has been achieved at low charge–discharge rates, low efficiency at high density current values restricts their performance [17]. This situation is a consequence of two factors: the low mobility of the electrolyte ions into the complex AC pore structure and the presence of Faradaic reactions in the surface oxygenated acidic groups (SOAG) inherent to the AC nature. Hence, the surface chemistry of the AC is also a relevant parameter.

Bamboos are a group of woody perennial plants in the grass family *Poaceae*, subfamily *Bambusoideae* [18]. Bambusa family *species: Vulgaris, Cacharensis, Arundinacea* and *Balcooa* from Asia, have shown high production of useful amount of biomass (more than 83 Tn/ha) [19,20]. On the other hand, *Guadua Angustifolia* species represents an endemic bamboo resource in some countries of South America [21].

The *Castanea sativa* [22] and *Juglans regia* [23] are two species of trees widely extended along Europe highly valued by their fruits (chestnuts and walnuts respectively); however the wastes derived from their consumption have not been exploited by industry.

In this manuscript, we describe the use of four abundant natural plant resources: *Guadua Angustifolia, Bambusa Vulgaris Striata (both from Veracruz-Mexico), Castanea Sativa* and *Juglans Regia* as activated carbon precursors. Scanning electron microscopy (SEM) has been used in order to observe their morphology, transmission electron microscopy (TEM) and associated techniques were

* Corresponding author. Fax: +34 913944352.
E-mail address: pegonzal@quim.ucm.es (P. González-García).

0169-4332/$ – see front matter © 2012 Elsevier B.V. All rights reserved.
http://dx.doi.org/10.1016/j.apsusc.2012.11.092

employed to analyze the nanostructure, chemical composition and the nature of bonding of the obtained materials. Their surface area and pore structure were also analyzed. Finally, their performance as electrodes in EDLC materials was evaluated. To the best of our knowledge, the use of the natural plant resources mentioned above as activated carbon precursors, have not been previously described in the literature.

2. Materials and methods

2.1. Sample carbonization and activation

Precursors *Guadua Angustifolia, Bambusa Vulgaris Striata (both from Veracruz-Mexico), Castanea Sativa* and *Juglans Regia (both from Galicia-Spain)* were reduced to 1 cm length. These particles were placed into a quartz crucible and heated at 400 °C in a tubular furnace under Ar atmosphere in order to remove their low boiling and melting point organic compounds. Finished the carbonization process, heating was turned off and the system was cooled down to 25 °C.

Carbons obtained from the previous stage were chemically activated with KOH by using the impregnation method. Samples were mixed by stirring for 120 min at 70 °C, with 10 ml of a solution containing the KOH/C ratio of 4:1. The resulting slurry was later on dried at 110 °C. The thermal activation treatment was also carried out in a tubular furnace under Ar atmosphere, during 60 min at 700 °C. Elapsed the activation time, heating was turned off and the system was cooled until 25 °C. Carbons obtained from this stage, were washed in a 0.1 M HCl solution and with distilled water until the total elimination of chlorine ions (detected via precipitation method with $AgNO_3$ 1 M solution). The final products were dried in a furnace at 110 °C during 24 h.

In order to label the produced activated carbons, the following nomenclature will be used: capitals CAC (chemically activated carbon) followed by the first letters corresponding to the precursor gender and species, for instance CACJR refers to the Activated Carbon produced from *Juglans Regia.*

2.2. Structural characterisation

Scanning electron microscopy (SEM) micrographs were obtained with a JSM 6335 F electron microscope operating at 10 kV and a working distance of 15 mm. Transmission electron microscopy (TEM) studies have been performed in a JEOL 3000 F (acceleration voltage of 300 kV) microscope (point resolution of 1.7 Å) equipped with an ENFINA spectrometer for Electron Energy Loss Spectroscopy (EELS) measurements. The EEL spectra were acquired in diffraction mode, with an acquisition time of 2 s, an energy dispersion of 0.1 eV/pixel (energy resolution 1.2 eV) and $\beta = 1.7$ mrad. This collection semi-angle value was chosen as close as possible to the "magic angle" [24] for C-K edge to avoid orientation effects on the spectra. Information about the local bonding nature of the carbon samples was obtained by EELS. From the high-loss region (higher than 50 eV), the carbon-K edge energy-loss near edge structure (ELNES) was employed for the quantification of the sp^2/sp^3 bonding ratio. The relative sp^2 content was estimated from the following expression [25]:

$$\frac{sp^2}{sp^2+sp^3} = \frac{\frac{I^s_{\pi*}}{I^s_{\pi*}+I^s_{\sigma*}}}{\frac{I^g_{\pi*}}{I^g_{\pi*}+I^g_{\sigma*}}} \quad (1)$$

where I_{π^*} and I_{σ^*} represent the integrated intensities provided by the $1s \rightarrow \pi^*$ and $1s \rightarrow \sigma^*$ transition peaks in the sample (s) and in the graphite (g) used as reference according to the two–windows (centrally positioned) method (TWC) [26]. Carbon mass-density was extracted from the position of the maximum of the bulk ($\pi+\sigma$) plasmon peak (Ep) [27] at the low-loss region of the EEL spectra (0–50 eV energy loss) [28] according to the next equation:

$$\rho = \frac{M_C m^* \varepsilon_0}{4N_A \hbar^2 e^2} Ep^2 \quad (2)$$

where M_c is the carbon molar mass, N_A the Avogrado number, e the electron charge, $\hbar$ the Planck's constant, ε_0 the vacuum dielectric function and m^* is the effective electron mass defined as 0.87 m, where m is the free electron mass.

The ultimate analyses were carried out by the Microanalytical service of the Complutense University. The Infrared (IR) spectra were recorded on a FTIR Thermo Nicolet200 spectrometer with samples as KBr pellets in the 4000–400 cm^{-1} region.

2.3. Textural studies

The adsorption of N_2 (77 K) was determined with a *Micromeritics ASAP 2010* apparatus and the data were analyzed using its software package, leading to the BET area (S_{BET}). In a second step, the analysis of the N_2 adsorption isotherm by the Dubinin-Radushkevich (DR) equation led to the micropore volume (W_0) and the so-called characteristic energy (E_0) of the carbons. The latter is related to the average width (L_0) of locally slit-shaped micropores by L_0 (nm) = 10.8/(E_0–11.4 kJ/mol which leads to the surface area of the micropore walls S_{mi} ($m^2\ g^{-1}$) = 2000 W_0($cm^3\ g^{-1}$)/L_o(nm) [29].

Moreover, the comparison of the isotherm obtained on the given carbons with the data obtained for a non-porous carbon used as reference (carbon black *Vulcan-3*) provided information on the total pore volume (V_{tot}) and the external (non microporous) surface area S_e of the carbons [30,31]. The total surface area of the monolith was estimated from $S_{DR} = S_{mi} + S_e$. The comparison plot also allowed the determination of the total surface area S_{comp}. The total surface area was also estimated by the analysis of the isotherm by the comparison plot S_{comp} [31] and by the BET equation [30].

2.4. Electrochemical performance

Two-electrode capacitors were assembled in a Swagelok® system with pellets of around 10 mg in weight. The electrode was composed of 75 wt. % of carbon, 20 wt.% of polivinylidene fluoride and 5 wt.% of carbon black. 2 M H_2SO_4 aqueous solution was used as electrolyte. A glassy fibrous material played the role of separator. The electrochemical measurements involved galvanostatic charging-discharging cycles at current densities between 1 and 100 mA/cm^2 potentiostat-galvanostat *Autolab-Ecochimie PGSTAT 30*). The cell voltage ranged from 0 to 0.8 V.

3. Results

3.1. Morphology

The morphology of the precursors and the CAC was studied by means of SEM (Fig. 1). As it can be observed in the micrographs, a characteristic morphology associated to the cellulose fibers prevails in all the precursors, inherent to their nature. The CAC prepared from *Castanea Sativa* and *Juglans Regia* lose the morphology observed in their precursors, however, this effect is not detected in those CAC produced from *Bambusa Vulgaris Striata* and *Guadua Angustifolia*, where the original micelle-like morphology remains after the chemical activation process.

3.2. Micro-nanostructure

The studies corresponding to the micro-nanostructure from these CAC were performed by TEM and associated techniques. The

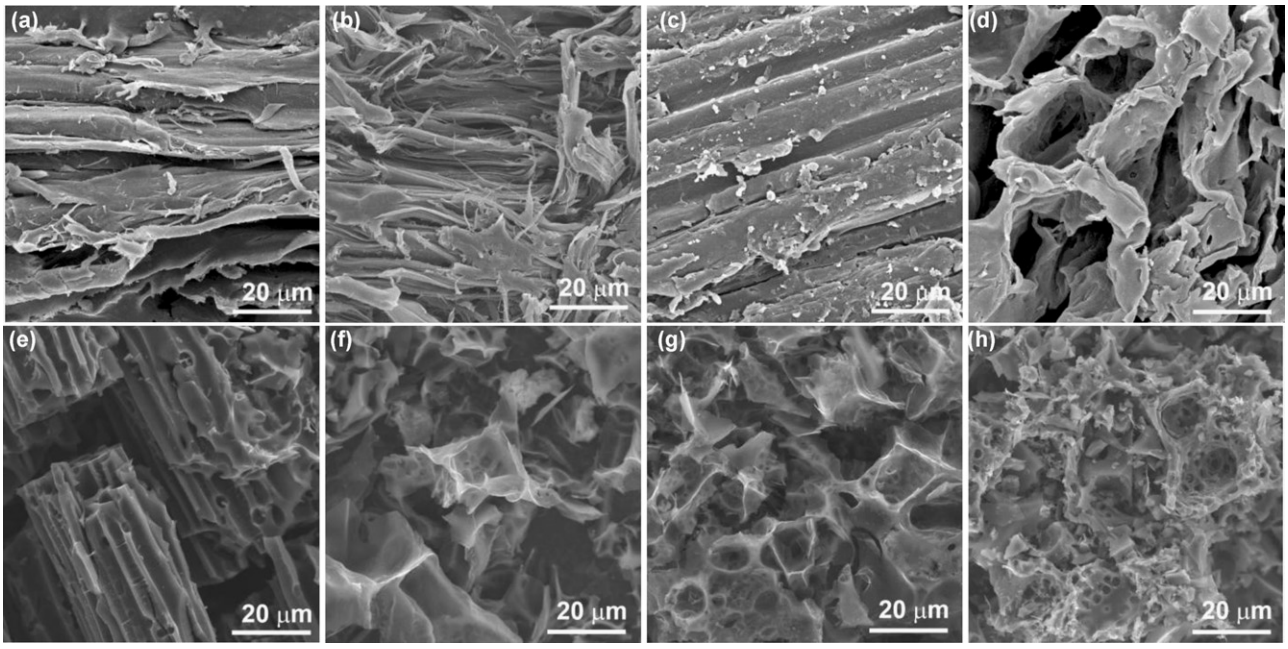

Fig. 1. SEM micrographs from the precursors (a) *Bambusa Vulgaris Striata*, (b) *Castanea Sativa*, (c) *Guadua Angustifolia*, (d) *Juglans Regia* and the products (e) CACBV, (f) CACCS, (g) CACGA and (h) CACJR.

low magnification and the High–Resolution TEM (HRTEM) images, displayed in Fig. 2, show that the CAC are formed by platelet–like particles with undefined morphology and variable dimensions and thickness. The contrast observed in their corresponding HRTEM images suggest that these CAC are formed by highly disordered graphene–like layers, as it can be confirmed with the very diffuse *hk0*–type diffraction rings in their Selected Area Electron Diffraction (SAED) patterns (see insets in Fig. 2a–d). The absence of the *00l* graphite–like reflections in the SAED, indicates that their nanostructure is highly disordered without tridimensional graphite–like stacking.

3.3. Density and proportion of sp^2 bonding content

Local information about the mass density and the sp^2/sp^3 bonding ratio from the CAC was obtained by using EELS. In the low–loss region (Fig. 3a) the π–π^* ($\sim$ 7 eV) and $\pi + \sigma$ ($\sim$ 27 eV) plamon peaks

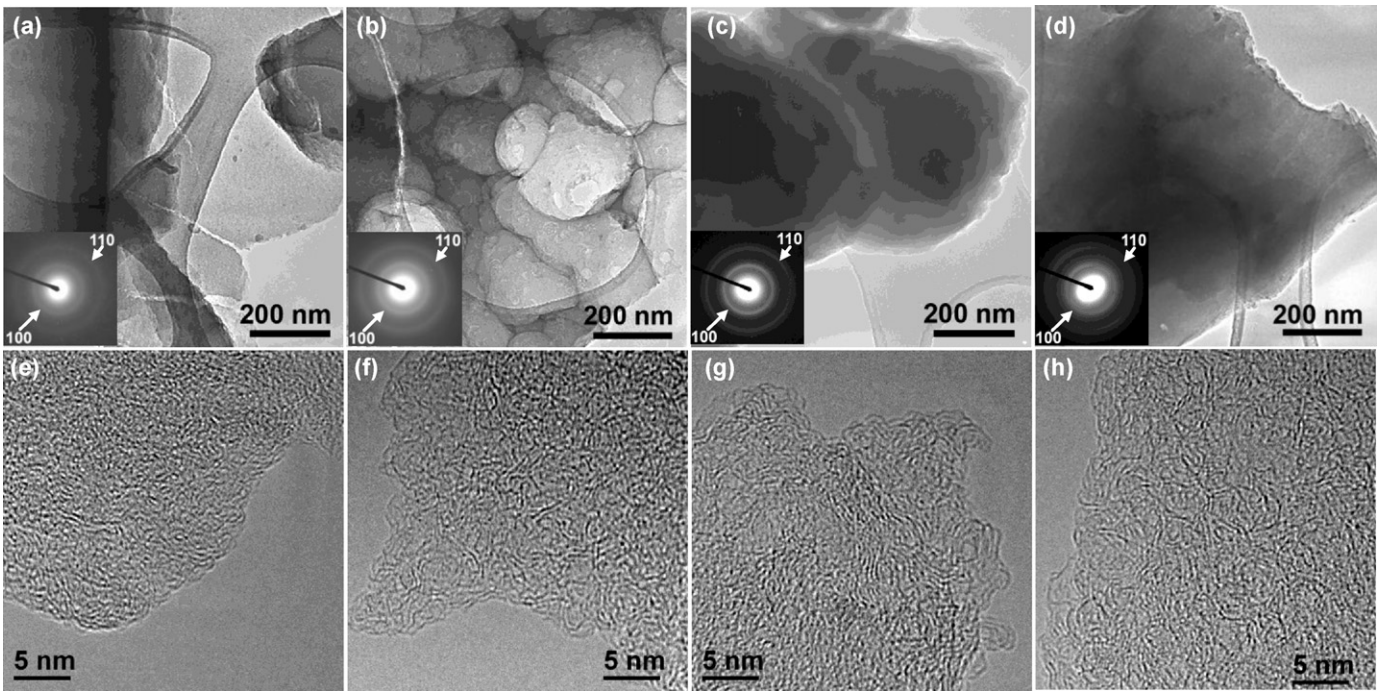

Fig. 2. Low magnification and High–Resolution TEM images, respectively from CACBV (a,e), CACCS (b,f), CACGA (c,g) and CACJR (d,h). Their corresponding SAED patterns are inset.

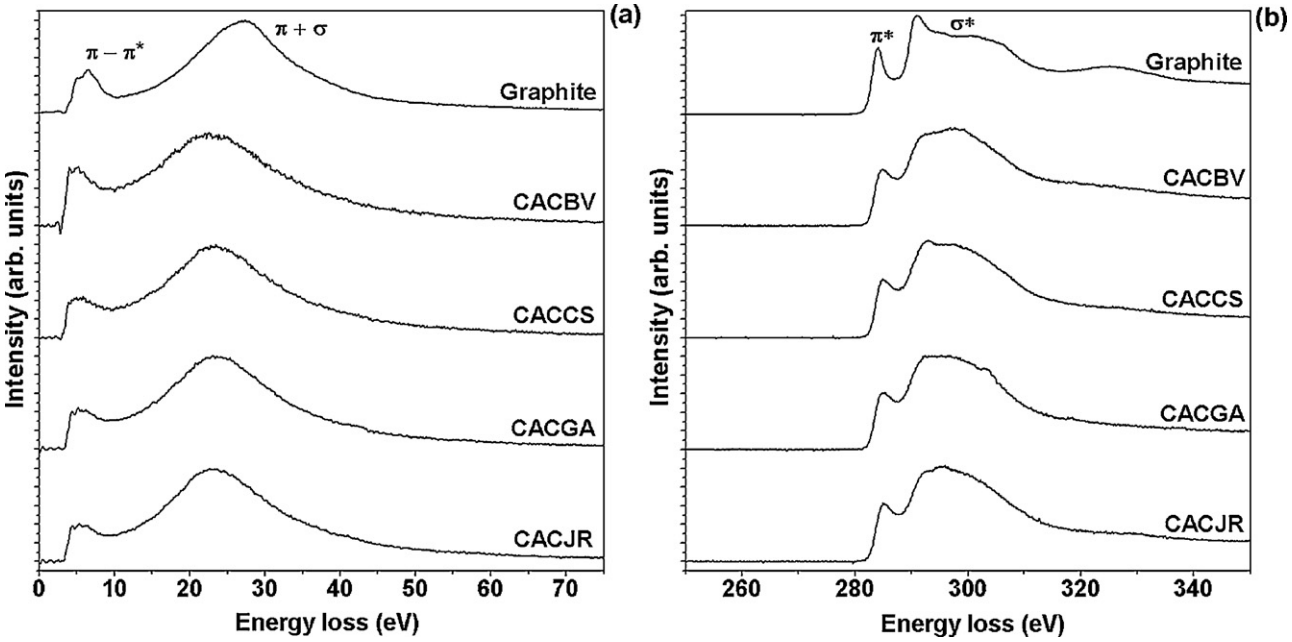

Fig. 3. EELS spectra from the CAC and the reference graphite in the low–loss region (a) and their carbon–K ELNES (b).

are detected and compared with those produced from the graphite used as reference.

In graphite, the π–π^* plamon is related to its band gap [32], therefore the close values of the π–π^* plamons position in the CAC and graphite (see Table 1) suggest a similar band gap. On the other hand, the position of the $\pi+\sigma$ plasmon is related to the mass density as it has been described by Ferrari et al. [27]. As it can be observed in Fig. 3a, the position of the maximum of the $\pi+\sigma$ plasmon of the CAC is located below the graphite one, yielding mass density values (see Table 1) 25% lower than graphite (2.2 g/cm^3) [33].

The carbon–K ELNES from the CAC and the reference graphite are represented in Fig. 3b. The CAC spectra show the same $1s \rightarrow \pi^*$ and $1s \rightarrow \sigma^*$ transition peaks (approximately at 284 and 291 eV) as in the reference graphite, nevertheless, the round and featureless σ^* maximum is characteristic of the highly disorder nature of the graphene–like layers in these materials, in agreement with the disordered structures detected by HRTEM (see Fig. 2). Their average sp^2 bonding content is 95% (see Table 1).

3.4. Surface chemistry

The chemical composition, derived from the proximal analysis of the raw materials and the CAC, are presented in Table 2. The precursors of this study have the characteristic composition of the lignocellulosic materials [4]. In comparison, the CAC present a carbon content higher than 80%.

Important concentrations of oxygen and hydrogen suggest the presence of high amount of surface oxygenated acidic groups (SOAGs) in the produced CAC. The semi–quantitative analyses performed by X–ray Energy Dispersive Spectroscopy (EDS), indicate a high content of oxygen (5–21%) in the CAC. However, as the EDS analysis is less sensitive for light elements ($Z \leq 10$) [34] the oxygen content was quantified by ultimate analysis (see Table 2). The oxygen concentrations quantified in these CAC, suggest the presence of high amount of diverse oxygenated groups on the carbon surfaces. The identification of the SOAGs was carried out by Infrared (IR) Spectroscopy (Fig. 4).

All the spectra present a sharp band in the range of 1615–1630 cm^{-1} indicating the presence of quinonic groups $\upsilon_{(C=O)}$, except in CACJR (Fig. 4d) where this band is broad and less defined. The bands situated at 1315 and 1380–1390 cm^{-1} due to the C–O stretching reveals the formation of xantenes $\upsilon_{(C-O)}$ and ethers $\upsilon_{(C-O)}$ groups, nevertheless a detailed observation allows to identify some differences in the last one. The presence of two bands (1050 and 1261 cm^{-1}) in CACBV (Fig. 4a) is indicative of asymmetric ethers (R–O–R′). In contrast a single band at 1070 cm^{-1} attributed to symmetric ethers (R–O–R) is observed in CACGA, CACCS and CACJR. The broad band observed in CACBV and CACGA at 3240 cm^{-1}, due to the H–O stretching, reveals also the presence of phenolic groups $\upsilon_{(H-O)}$.

The weak and broad bands in the range from 2850–2950 cm^{-1}, can be assigned to the asymmetric $\upsilon_{as(C-H)}$ and symmetric $\upsilon_{s(C-H)}$ C–H stretching, while the weak bands at 670 and 785 cm^{-1} correspond to the out–of–plane bending $\upsilon_{(C-H)}$ and scissoring $\gamma_{(C-H)}$, respectively.

Table 1
Parameters derived from the EELS spectra.

	π–π^* (eV)	$\pi+\sigma$ (eV)	$\rho \pm 0.1$ (g/cm^3)	$sp^2 \pm 3$ (%)
CACBV	6.6	23.1	1.6	94
CACCS	6.6	23.6	1.7	95
CACGA	6.6	23.7	1.7	95
CACJR	6.7	23.4	1.7	95
Graphite	7.2	26.9	2.2	100

Table 2
Ultimate analysis from the precursors and the CAC (%).

	C	H	N	O
Bambusa Vulgaris Striata	44.97	5.82	0.46	48.75
CACBV	84.61	3.47	0.56	11.36
Castanea Sativa	46.15	5.52	0.52	47.81
CACCS	83.16	3.58	0.87	12.39
Guadua Angustifolia	44.84	5.84	0.91	48.41
CACGA	82.85	2.88	1.22	13.05
Juglans Regia	48.08	6.11	0.30	45.51
CACJR	80.07	3.34	0.38	16.31

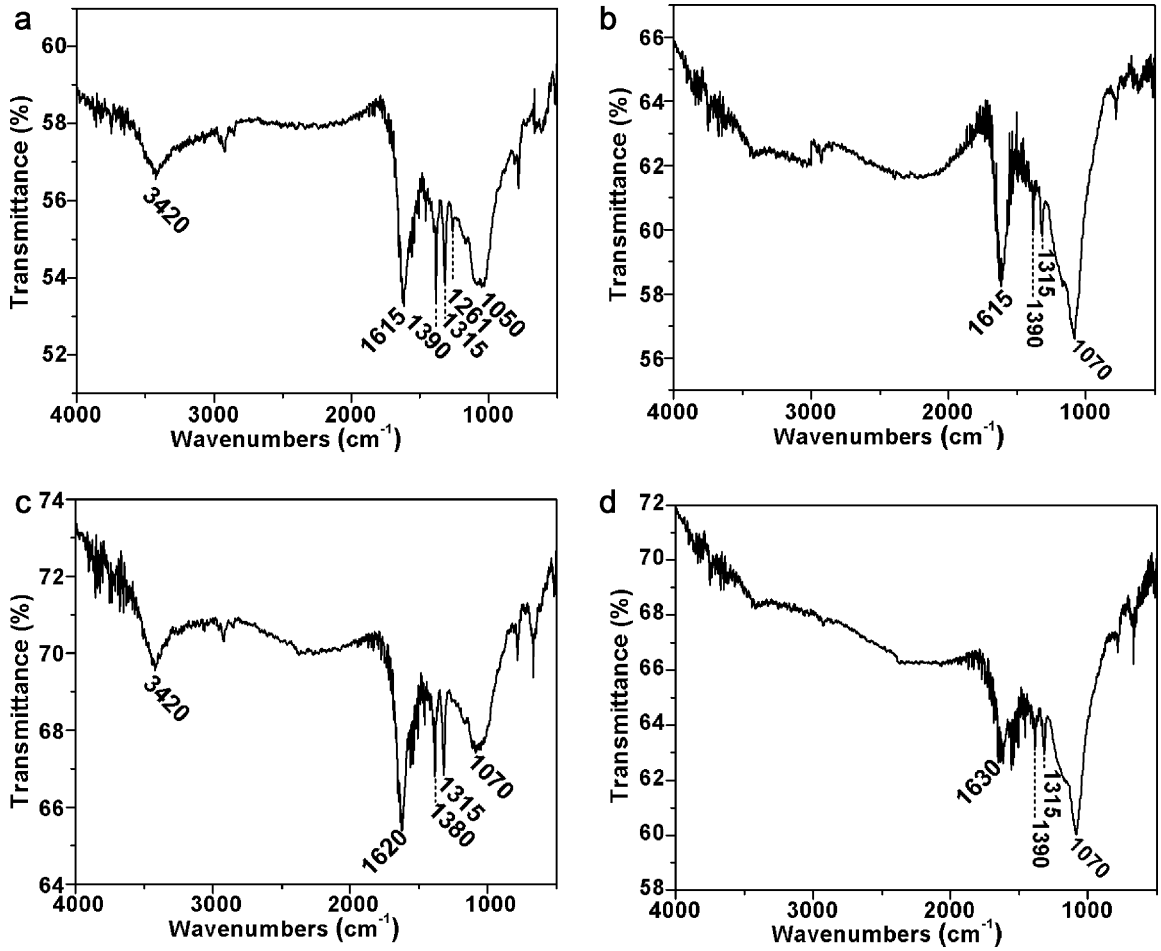

Fig. 4. Infrared spectra from CACBV (a), CACCS (b), CACGA (c) and CACJR (d).

3.5. Surface area and porous structure

An overview of the main porous properties of the CACs is provided by the results summarised in Table 3. The nitrogen adsorption–desorption measurements at 77 K on the CAC prepared in this work are displayed in Fig. 5. The isotherm plots follow the Type I according to the IUPAC classification [30]. It appears that the porosity of the present CACs consists mainly of micropores (width < 2 nm). Their microporous surface areas (S_{mi}) range from 826 m^2/g for CACCS to 1044 m^2/g for CACGA. All CAC- materials do not contain a significant proportion of larger pores which lead to external (non-microporous) surfaces areas (S_e) below 20 m^2/g.

The comparison of the textural parameters of carbons (Table 3) reveals a similar porous structure for materials derived from *Bambusa Vulgaris Striata*, *Castanea Sativa* and *Juglans Regia* (total pore volume V_{tot} around 0.77 cm^3/g and average micropore width L_0 between 1.30 and 1.38 nm) whereas a slight increase in the porosity development is observed when *Guadua Angustifolia* is used as precursor (total pore volume as high as 1.25 cm^3/g and micropores centered at around 1.80 nm).

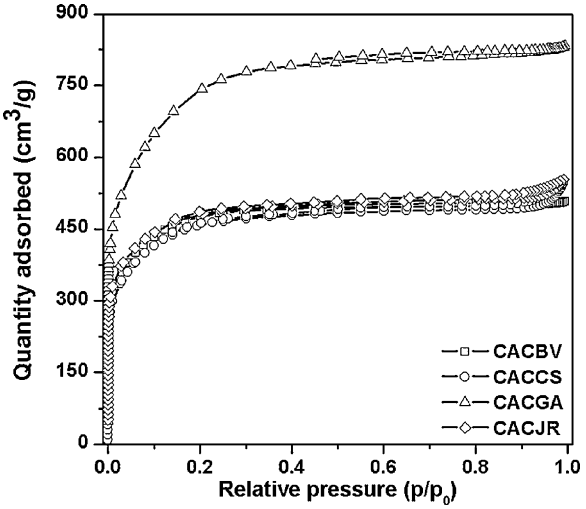

Fig. 5. N_2 adsorption–desorption isotherm plots for the CAC prepared at 700 °C.

Table 3
Characteristics of the porous structure of the CAC.

	V_{tot} (cm^3/g)	W_0 (cm^3/g)	L_0 (nm)	S_{mi} (m^2/g)	S_e (m^2/g)	$S_{DR} = S_{mi} + S_e$ (m^2/g)	S_{comp} (m^2/g)	S_{BET} (m^2/g)
CACBV	0.77	0.61	1.30	938	5	943	1054	1700
CACCS	0.74	0.57	1.38	826	20	846	860	1652
CACGA	1.25	0.94	1.80	1044	10	1054	1158	2555
CACJR	0.78	0.64	1.32	970	17	987	1031	1703

Table 4
Specific capacitance, C, per mass of carbon, from the CAC (F/g).

	Current density (mA/cm^2)									
	1	3	5	7	10	20	30	50	70	100
CACBV	156	149	145	137	123	106	93	54	47	-
CACCS	100	88	78	64	52	34	-	-	-	-
CACGA	154	151	149	147	138	118	94	68	-	-
CACJR	161	159	150	147	142	132	119	105	87	84

Table 3 shows the good agreement between S_{DR} and S_{comp} whereas S_{BET} greatly exceeds. Such a difference is not surprising because, as previously discussed by several authors [29,31,35], S_{BET} does not accurately represent the surface area in the case of highly microporous materials as the present CAC. Despite the lack of physical meaning, the values of S_{BET} are included in Table 3 to facilitate comparison of our materials with those shown in the literature. For the present case, the real total surface areas (estimated from the average total surface obtained by independent techniques, S_{DR} and S_{comp}) are between 850 and 1100 m^2/g which fit into the general pattern found for activated carbons produced from lignocellulosic wastes [3,36].

3.6. Electrochemical performance

The characteristics of the previously described CAC (nanostructure and porous structure) suggest their promising application as electrode materials in EDLC devices. It has been tested in a galvanostatic charge–discharge system with current density (d) in the range from 1–100 mA/cm^2. As reported in Table 4, specific capacitances above 100 F/g are achieved for the present CAC at low current density (1 mA/cm^2). In the case of CACJR, a value as high as 161 F/g is reached. These results match and even surpass the values quoted in the literature for AC derived from lignocellulosic precursors, such as: coffee endocarp [13] or cherry stones [36]. At high current density, the specific capacitance markedly decreases. Such behaviour has been observed for carbons with high oxygen content which is the case for the present materials. As summarized in Table 2, these CAC have important oxygen concentrations forming the SOAGs previously identified by IR (see Fig. 4). These oxygenated surface functionalities increase the overall capacitance at low current density by the contribution of pesudocapacitive processes to be added to the double-layer mechanism. On the other hand, they are also responsible of the drop in the capacitance at high current densities [12,17,36]. As already reported, this drawback may be surpassed by post-heat treatment of carbons under inert atmosphere at temperatures above 800 °C [37].

4. Summary and conclusions

In the present work we propose the use of abundant lignocellulosic precursors: *Guadua Angustifolia*, *Bambusa Vulgaris Striata*, *Castanea Sativa* and *Juglans Regia* for the synthesis of activated carbon via chemical activation. Although the impregnation process with KOH is almost a quite established method for the preparation of highly microporous carbons, the use of low cost precursors, based in waste materials, offers significant alternatives for their production.

The produced CAC are composed by a nanostructure formed by highly disordered graphene–like layers, sp^2 bonding content average of 95% and mass density 25% below than the standard graphite. The textural studies show real total surface areas ranging from 850 to 1100 m^2/g and average micropore widths between 1.30 and 1.80 nm, making them promising candidates for diverse applications, especially for energy–related materials such as fuel cell systems, lithium–ion batteries, etc. In this context, we have found specific capacitance as high as 100–161 F/g.

The highest specific capacitance value at low current density was observed in CACJR (161 F/g); however, this significant behavior has not been only attributed to its textural features: surface area around 1000 m^2/g and average pore width L_0 = 1.32 nm, since we have identified the presence of pseudocapacitance in the electrode as consequence of its high content of oxygen as quinonic and ether groups. Hence, the possibility of tuning the surface chemistry of the present CAC in order to enhance their performance presents perspectives for future work.

Acknowledgements

The authors would like to thank the financial support through the projects with references S-2009/PPQ-1626 and MAT2010-19460. P. González-García would like to thank CONACYT (Mexico) for a Ph. D. grant.

References

[1] J.M. Dias, M.C.M. Alvim-Ferraz, F.M. Almeida, J. Rivera-Utrilla, M. Sánchez-Polo, Waste materials for activation carbon preparation and its use in aqueous-phase treatment: a review, Journal of Environment Management 85 (2007) 833–846.
[2] M.O. Abdullah, I.A.W. Tan, L.S. Lim, Automobile adsorption air-conditioning system using oil palm biomass-based activated carbon: A review, Renewable and Sustainable Energy Reviews 15 (2011) 2061–2072.
[3] O. Ioannidou, A. Zabaniotou, Agricultural residues as precursors for activated carbon production-A review, Renewable and Sustainable Energy Reviews 11 (2007) 1966–1975.
[4] H. Marsh, F. Rodriguez-Reinoso, Activated carbon, Elsevier Ltd, Oxford UK, 2006.
[5] M. Mochida, B. Fotoohi, Y. Amamo, L. Mercier, Cadmium (II) and lead (II) adsorption onto hetero-atom functional mesoporous silica and activated carbon, Applied Surface Science 258 (2012) 7389–7394.
[6] Rodríguez, J. García, G. Ovejero, M. Mestanza, Adsorption of anionic and cationic dyes on activated carbon from aqueous solutions: equilibrium and kinetics, Journal of Hazardous Materials 172 (2009) 1311–1320.
[7] V.I. Águeda, B.D. Crittenden, J.A. Delgado, S.R. Tennison, Effect of channel geometry, degree of activation, relative humidity and temperature on the performance of binderless activated carbon monoliths in the removal of dichloromethane from air, Sep. Purif. Technol. 78 (2011) 154–163.
[8] B. Petrova, T. Budinova, B. Tsyntsarski, V. Kochcodan, Z. Shkavro, N. Petrov, Removal of aromatic hydrocarbons from water by activated carbon from apricot stones, Chemical Engineering Journal 165 (2010) 258–264.
[9] C. Pevida, M.G. Plaza, B. Arias, J. Fermoso, F. Rubiera, J.J. Pis, Surface modification of activated carbons for CO_2 capture, Applied Surface Science 254 (2008) 7165–7172.
[10] J. Skubiszewska-Zieba, VPO catalysts synthesized on substrates with modified activated carbons, Applied Surface Science 256 (2010), 5520–2257.
[11] M. Fernández, J. Valenciano, F. Trinidad, N. Muñoz, The use of activated carbon and graphite for the development of lead-acid batteries for hybrid vehicle applications, Journal of Power Sources 195 (2010) 4458–4469.
[12] E. Frackowiak, F. Béguin, Carbon materials for the electrochemical storage of energy in capacitors, Carbon 39 (2001) 937–950.
[13] M. Selvakumar, D.K. Bhat, Microwave synthesized nanostructured TiO_2-activated carbon composite electrodes for supercapacitor, Applied Surface Science (2012) http://dx.doi.org/10.1016/j.apsusc.2012.09.036
[14] E. Frackowiak, F. Béguin, Nanotextured carbons for electrochemical energy storage, in: Y. Gogotsi (Ed.), Nanomaterials Handbook, CRC, Press, Boca Raton FL, 2006, pp. 713–734.
[15] T.A. Centeno, F. Stoeckli, The role of textural characteristics and oxygen-containing surface groups in the supercapacitor performances of activated carbons, Electrochimica Acta 52 (2006), 560–566.
[16] M. Inagaki, H. Konno, O. Tanaike, Carbon materials for electrochemical capacitors, Journal of Power Sources 195 (2010) 7780–7903.

[17] T.A. Centeno, F. Stoeckli, On the specific double-layer capacitance of activated carbons, in relation to their structural and chemical properties, Journal of Power Sources 154 (2006) 314–320.
[18] M. Krzesinska, B. Pilawa, S. Pusz, J. Nh, Physical characteristics of carbon materials derived from pyrolysed vascular plants, Biomass and Bioenergy 30 (2006) 166–176.
[19] P. Shanmughavel, R.S. Peddappaiah, T. Muthukumar, Biomass production in an age series of Bambusa bamboos plantations, Bioresource Technology 20 (2001) 113–117.
[20] A.J. Nath, G. Das, A.K. Das, Above ground standing biomass and carbon storage in village bamboos in North East India, Biomass and Bioenergy 33 (2009) 1188–1196.
[21] J. Olivier, T. Otto, M. Roddaz, P.O. Antoine, X. Londoño, L.G. Clarck, First macrofossil evidence of a pre-Holocene thorny bamboo cf. Guadua (Poaceae: Bambusoideae: Bambuseae: Guaduinae) in south-western Amazonia (Madre de Dios – Peru), Review of Palaeobotany and Palynology 153 (2009) 1–7.
[22] J. Fernández-López, R. Alía-Miranda, Guía técnica para la conservación genética y utilización del Castaño (*Castanea Sativa*), Eurogen, Madrid, 2008.
[23] B. Fornari, F. Cannata, M. Spada, M.E. Malvolti, Allozyme analysis of genetic diversity and differentiation in European and Asiatic walnut (*Juglans regia L.*) populations, Forest Genetics 6 (1999) 115–127.
[24] H. Daniels, A. Brown, A. Scott, T. Nichells, B. Rand, R. Brydson, Experimental and theoretical evidence for the magic angle in transmission electron energy loss spectroscopy, Ultramicroscopy 96 (2004) 523–534.
[25] A.C. Ferrari, B. Kleinsorge, G. Adamopoulos, J. Robertson, W.I. Milne, V. Stolojan, Determination of bonding in amorphous carbons by electron energy loss spectroscopy, Raman scattering and X-ray reflectivity, Journal of Non-crystalline Solids 266 (2000) 765–768.
[26] N. Bernier, F. Bocquet, A. Allouche, W. Saikaly, C. Brosset, J. Thibault, A methodology to optimize the quantification of sp^2 carbon fraction from K edge EELS spectra, Journal of Electron Spectroscopy and Related Phenomena 164 (2008) 4–43.
[27] A.C. Ferrari, A. Libassi, B.K. Tanner, V. Stolojan, J. Yuan, L.M. Brown, Density, sp^3 fraction, and cross-sectional structure of amorphous carbon films determined by x-ray reflectivity and electron energy-loss spectroscopy, Physical Review B 62 (2000) 11089–11103.
[28] R.F. Egerton, Electron energy-loss spectroscopy in the electron microscope, Plenum Press, New York, 1996.
[29] T.A. Centeno, F. Stoeckli, The assessment of surface areas in porous carbons by two model-independent techniques, the DR equation and DFT, Carbon 48 (2010) 2478–2486.
[30] S.J. Gregg, K.S.W. Sing, Adsorption, surface area and porosity, Academic Press, London, 1982.
[31] N. Setoyama, T. Susuki, K. Kaneko, Simulation study on the relationship between a high resolution α_s-plot and the pore size distribution for activated carbon, Carbon 36 (1998) 1459–1467.
[32] T. Hanada, Y. Okada, K. Yase, Structure of multi–walled and single–walled carbon nanotubes, in: K. Tanaka, T. Yamabe, K. Fukui (Eds.), EELS study, The science technology of carbon nanotubes, Elsevier Ltd, Oxford, U.K., 1999, pp. 29–39.
[33] N.N. Greenwood, A. Earnshaw, Chemistry of the Elements, 1st Ed., Pergamon press, U.K, 1984.
[34] D.B. Williams, C.B Carter, Transmission Electron Microscopy. Chap 1, 2nd Ed., Plenum Publishing Co., New York, 2009.
[35] F. Stoeckli, A. Guillot, A.M. Slasli, D. Hugi-Cleary, Microporosity in carbon blacks, Carbon 40 (2002) 211–215.
[36] M. Olivares-Marín, J.A. Fernández, M.J. Lázaro, C. Fernández-González, A. Macías-García, V. Gómez-Serrano, Cherry stones as precusor of activated carbons for supercapacitors, Materials Chemistry and Physics 114 (2009) 323–327.
[37] J. Sánchez-González, F. Stoeckli, T.A. Centeno, The role of the electric conductivity of carbons in the supercapacitor performance, Journal of Electroanalytical Chemistry 657 (2001) 176–180.